International Journal of Engineering Science Invention

Volume 2 Issue 1 ‖ January. 2013

A comparative study on dynamic optical filtering and temperature sensing capabilities between 1D binary and ternary photonic crystals

Avisek Lahiri [1*], Manashi Chakraborty[2]

Department of Electronics and Communication Engineering, Institute of Engineering and Management, Kolkata, India

ABSTRACT: *In this paper a comparative study has been performed between 1D binary and ternary PHC (photonic crystal) on their capabilities as dynamic optical filter and a temperature sensor. The binary crystal consists of periodic alignment of alternate layers of 500nm thick GaAs slabs separated by air while the ternary PHC consists of periodic arrangement of GaAs, InAs and air layers. The study is restricted between 800nm-4000nm of the electromagnetic spectrum while the temperature swing is kept between 100-700K. The binary PHC shows four optical band gaps compared to seven band gaps by its ternary counterpart. The rejection factor evaluated at the central forbidden wavelength has been taken as the figure of merit for optical filtering and temperature sensing. Both for binary and ternary PHC, except for bandgap-1 of binary PHC and bandgap-1&2 of ternary PHC, the temperature sensing becomes more effective as temperature is increased from 100K to 700K. The binary crystal outperforms the ternary crystal as a temperature sensor when the working range of the incident wave is between 840nm-1100nm, after which the ternary PHC's performance outweighs the binary PHC. The dynamic optical filtering has been studied by fixing temperature at 300K and varying the angle of incidence the ray incident on the crystal from 0°-32°, as at 32° the relative attenuation of the optical power from allowable band comes out to be 3dB. At constant temperature(300K) the selective rejection capacity of ternary PHC was superior to binary PHC . The binary PHC works better than the ternary PHC in the range of 820nm-900nm after which the ternary crystal is more effective as dynamic optical filter than the binary PHC.*

Keywords—*Photonic crystals, reciprocal lattice, Brillouin zone, photonic bandgap, optical tuner, temperature sensor, Chebyshev polynomials*

I. INTRODUCTION

The celebrated papers of Yablonovitch [1-2] and John [3] opened up the horizons for the field of photonic crystal (PHC). Ever since then, the field of PHC has been a favored area of research. PHC is a 3D crystal with periodic repetition of refractive index profile. According to the dimensionality of periodicity a PHC can be classified as 1D, 2D or 3D [4]. The mathematical relation between frequency (ω) of incident wave and the wave vector (k) exhibits a band structure. Analogous to the Brillouin zones found in semiconductor physics [5], a PHC also exhibits the presence of several Brillouin zones. The III-V class of semiconductors especially those having refractive index greater than 2.0 are favored materials for photonic crystals [6]. The close analogy of optical bandgap with electronic bandgap [7] has been applied in various fields of study like optical tuner, omnidirectional

Avisek Lahiri Address: Gurukul, Y-12, Block -EP, Sector-V, Salt Lake, Kolkata-91, India

Reflectors [8-11] etc. Optical tuner is an essential component for optical communication systems. The fact that dynamic optical tuning is temperature dependant and that this principle can be applied for implementing a temperature sensor has been illustrated in [12]. The characteristics matrix mathematical approach has been used to perform a comparative study between 1D binary and ternary PHC as dynamic optical tuner and temperature sensor. The binary PHC consists of alternate arrangement of GaAs and air layers while the ternary PHC consists of GaAs, InAs and air layers in alternation. At first the mathematical formulation has been discussed in short after which we compare the dynamic optical filtering performance by keeping temperature constant at 300K and varying the angle of incidence from 0°- 32°. In the next section we evaluate the temperature sensing performance by keeping the angle of incidence fixed at 0° and varying the temperature from 100K-700K.

II. MATHEMATICAL FORMULATION

Fig. 1 shows the arrangement of 1D binary and ternary PHC. The refractive index is periodic along the Z axis. For the binary crystal the refractive index profile is given by

$\eta(z)= \eta_1$ for 0<z<d1
$= \eta_2$ for d1<z<d2

While for the ternary crystal the refractive index profile is given as

$\eta(z)= \eta_1$ for 0<z<d1
$= \eta_2$ for d1<z<d2
$= \eta_3$ for d2<z<d3

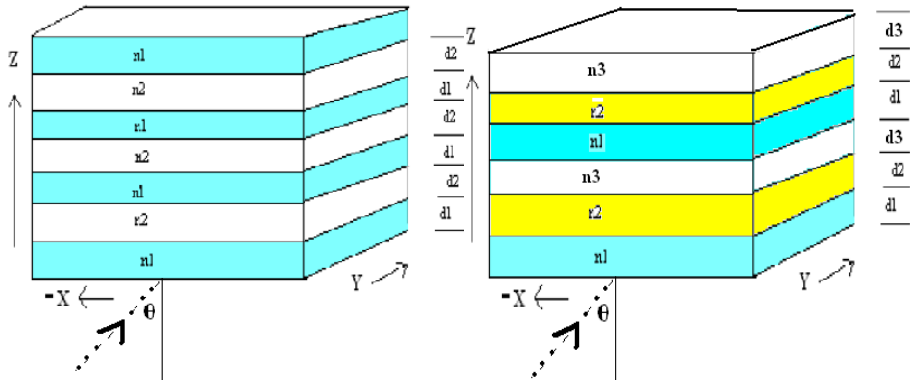

(1.a) **(1.b)**

Figure 1. Representation of 1D binary (1.a) and ternary PHC (1.b)

In this kind of arrangement, $\eta(z)= \eta(z+D)$, where "D" is the periodicity of the crystal. According to the mathematical formulation laid down in [13], for a multi layered structure as in Fig.1, the characteristic matrix for one period and a TE polarized incident wave is given as :

$$M(D)=\prod_{i=1}^{i=k}. \begin{pmatrix} \cos\gamma_i & -i\sin(\gamma_i)/p_i \\ -ip_i\sin(\gamma_i) & \cos(\gamma_i) \end{pmatrix} \quad (1)$$

Where,

$$\gamma_i = \frac{2\pi\eta_i\cos\theta_i}{\lambda} \quad (2)$$

$$\cos\theta_i = \sqrt{1-\frac{\sin^2\theta}{\eta_i^2}} \quad (3)$$

$p_i= \eta_i*\mathrm{Sin}(\theta_i)$ (4)

θ_i is the angle made by the wave in the (i^{th}) layer with the normal and (θ) is the angle of incidence of the ray. For the binary PHC k=2 and for the ternary PHC k=3 and (λ) is the incident wavelength. For the binary crystal, Equation (1) can be formulated as

$$M(D) = \begin{matrix} m_{11} & m_{12} \\ m_{21} & m_{22} \end{matrix} \quad (5)$$

where,

$$m_{11} = \cos\gamma_1\cos\gamma_2 - \frac{p_2\sin\gamma_1\sin\gamma_2}{p_1} \quad \ldots(6)$$

$$m_{12} = -i\left(\frac{\cos\gamma_1\sin\gamma_2}{p_2} + \frac{\sin\gamma_1\cos\gamma_2}{p_1}\right) \quad \ldots (7)$$

$$m_{21} = -i(p_1\sin\gamma_1\cos\gamma_2 + p_2\sin\gamma_2\cos\gamma_1) \quad \ldots(8)$$

$$m_{22} = \cos\gamma_1\cos\gamma_2 - \frac{p_1\sin\gamma_1\sin\gamma_2}{p_2} \quad \ldots(9)$$

Similarly for the ternary crystal, the characteristic matrix of one period is expanded as (4), where

$$m_{11} = \cos\gamma_3\left(\cos\gamma_1\cos\gamma_2 - \frac{p_2\sin\gamma_1\sin\gamma_2}{p_1}\right) - p_3\sin\gamma_3\left(\frac{\cos\gamma_1\sin\gamma_2}{p_2} + \frac{\sin\gamma_1\cos\gamma_2}{p_1}\right) \quad \ldots\ldots \quad (10)$$

$$m_{12} = i\left[\frac{\sin\gamma_1\cos\gamma_2\cos\gamma_3}{p_1} + \frac{\cos\gamma_1\sin\gamma_2\cos\gamma_3}{p_2} + p_1\cos\gamma_1\cos\gamma_2\sin\gamma_3 - \frac{p_2\sin\gamma_1\sin\gamma_2\gamma_3}{p_1^2}\right] \quad \ldots. \quad (11)$$

$$m_{22} = \frac{-\sin\gamma_3[p_1 \sin\gamma_1 \cos\gamma_2 + p_2 \cos\gamma_1 \sin\gamma_2]}{p_3} + \cos\gamma_3[\cos\gamma_1 \cos\gamma_2 - \frac{p_1 \sin\gamma_1 \sin\gamma_2}{p_2}] \quad \ldots\ldots \quad (12)$$

$$m_{21} = -i[p_1 \sin\gamma_1 Cos\gamma_2 \cos\gamma_3 + p_2 \cos\gamma_1 \sin\gamma_2 \cos\gamma_3 + p_1 \cos\gamma_1 \cos\gamma_2 \sin\gamma_3 - \frac{p_1^{\,2} \sin\gamma_1 \sin\gamma_2 \sin\gamma_3}{p_2}] \quad \ldots(13)$$

For a crystal consisting on (N) periods the overall characteristic matrix is given by $M(N(D))=M(D)^N$., where

$$M(D)^N = \begin{vmatrix} m_{11}U_{N-1}(a) - U_{N-2}(a) & M_{12}U_{N-1}(a) \\ m_{21}U_{N-1}(a) & m_{22}U_{N-1}(a) - U_{N-2}(a) \end{vmatrix} \quad (14)$$

where: $a=0.5*(m_{11}+m_{22})$

$U_N(a) = \frac{\sin((N+1)\cos^{-1}(a))}{\sqrt{1-a^2}}$ are the Chebyshev polynomials in (a) and is a real quantity. The band structure of the PHC is dependent on the transfer matrix as given in Equation(5) and for that we need to concentrate on the eigen values of the characteristic matrix of one period which is given by

$\det[M(d)-\lambda I]=0$ (15)

or, $\lambda=a\pm(a^2-1)^{0.5}$ (16)

Solution to Equation (16) is given by taking a=cos(t). Thus whenever |a|<=1, we have an allowable band else we have a bandgap.

III. VARIATION OF THERMAL EXPANSION COEFFICIENT AND REFRACTIVE INDEX

Solution to Equation (16) is dependent on refractive index(η) and lattice dimensions which are dependent on temperature. Hence corrections need to be incorporated regarding this factor. For GaAs and InAs the variation of thermal expansion coefficient has been illustrated by Glazov and Pashinkin [14] as

$$\frac{\Delta l}{l_{GaAs}} = -1.3659*10^{-3} + 4*10^{-6}T + 1.0*10^{-9}T^2$$

$$\frac{\Delta l}{l_{InAs}} = -1.201*10^{-3} + 3.45*T*10^{-6} + 9.78*T^2*10^{-10}$$

The refractive index variations of InAs[15] and GaAs[16] are given by

$$\eta_{InAs} = 3.4165 + 9.05*T*10^{-5} + 7.05*T^2*10^{-7} - 7.46*T^3*10^{-10}$$

$$\eta_{GaAs} = 3.255*(1 + 4.5*T*10^{-5})$$

IV. VARIATION OF LATTICE PARAMETERS DUE TO TEMPERATURE CHANGE

In this section the variation of thickness of individual layers due to change of temperature has been studied. Fig.2 shows the change in lattice dimensions with the variation of temperature. d1,d2 and d3 are the initial thickness of GaAs, InAs and air layers respectively. We have taken into assumption that there is no expansion at the GaAs and InAs junction as that will lead to localized defects formation. With this consideration the new lattice dimensions become, d1'=d1+Δl1, d2'=d2+Δl2 and d3'=d3-(Δl1+Δl2). For binary PHC the new lattice dimensions are: d1'=d1+ Δl1 and d2'=d2-Δl1 as depicted in Fig. 2.b. These changes need to be incorporated in Equation (5) for getting proper band structure at different temperatures.

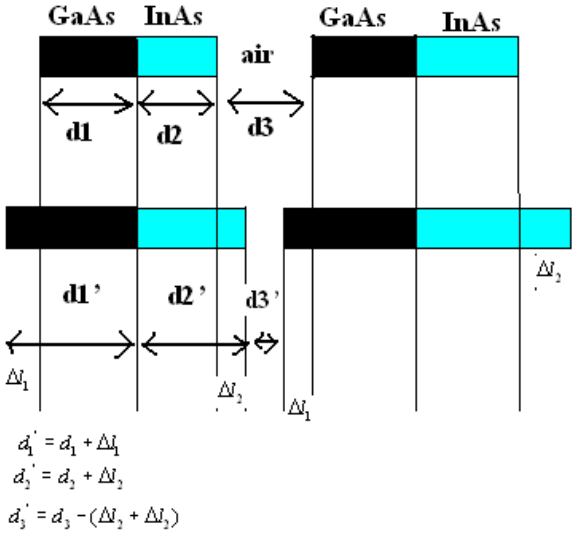

Figure 2.a Pictorial representation of variation in lattice parameters With change in temperature in ternary PHC

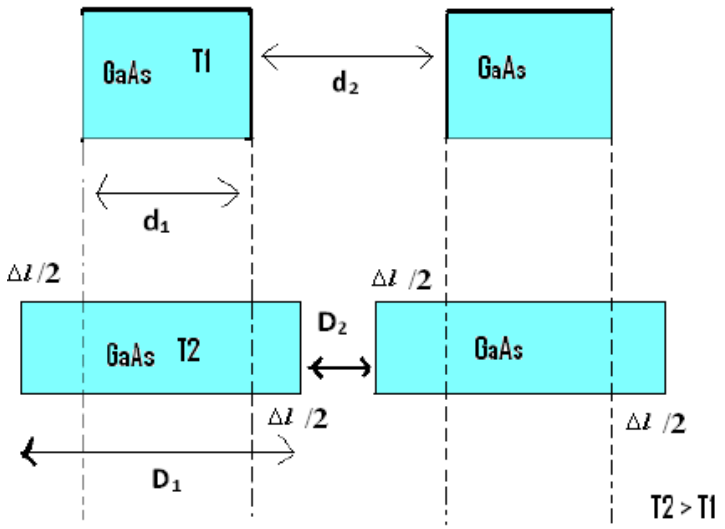

Figure 2.b Pictorial representation of variation in lattice Parameters with change in temperature in binary PHC

V. RESULT COMPARISON WITH FDTD (Finite Difference Time Domain)

We first verified our mathematical model by simulating the band structure for a 1D binary PHC at 300K and normal angle of incidence. The material parameters were as follows:

η_1=3.299 (GaAs) η_2= 1 (Air)

$d_1 = d_2$= 500nm

The band structure was evaluated with the help of MATLAB simulation. Fig.3 shows the positions of bandgaps where |a|= | Cos t| > 1.

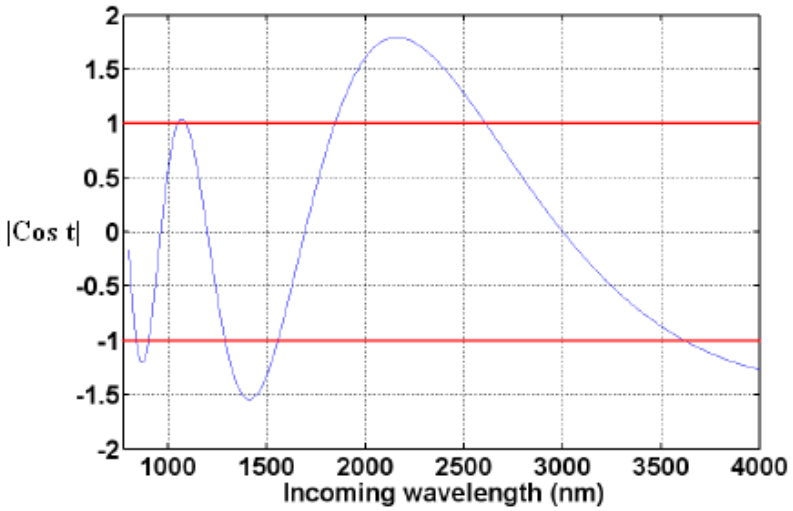

Figure 3. Band structure for 1D binary PHC

The above plot shows that a PHC is capable of opening up of bandgap and in this case the bandgaps are located at 838nm≤λ≤901nm, 1048nm≤λ≤1091nm, 1289nm≤λ≤1557nm, 1846nm≤λ≤2601nm .

Our results were then verified by simulating the band structure using OptiFDTD version 10 software. Fig. 4.a shows the fabrication layout of the crystal in the simulator. The blue lines represent GaAs layers separated by air layers. Fig. 4.b depicts the band structure as evaluated by the simulator using FDTD approach. We need to take the inverse of the coordinates as specified in the band structure of the simulation results which gives the bandgap range in micrometer scale. So, we need to convert the range to nanometer scale before comparing with our modeled results.

Bandgap #1 stretches from 1289nm-1556 nm

Bandgap #2 stretches from 1854nm-2574nm which matched with our modeled band structure.

In accordance to the OptiFDTD manual [17], our modeling evaluated two more bandgaps compared to the band structure computed by FDTD approach.

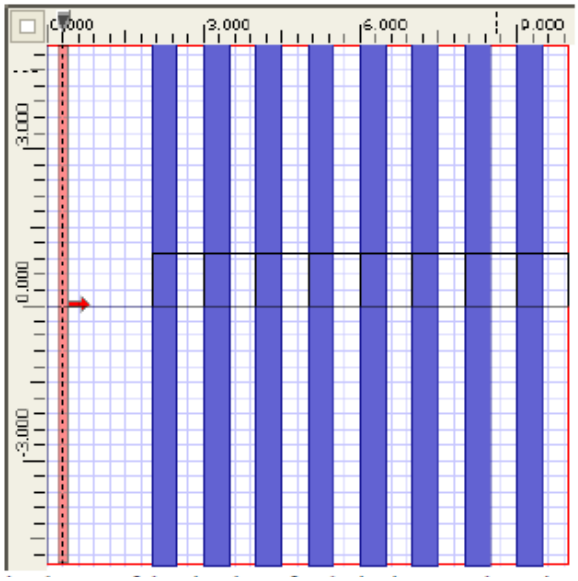

Figure 4.a Fabrication layout of 1D binary PHC in OptiFDTD 10.0 software

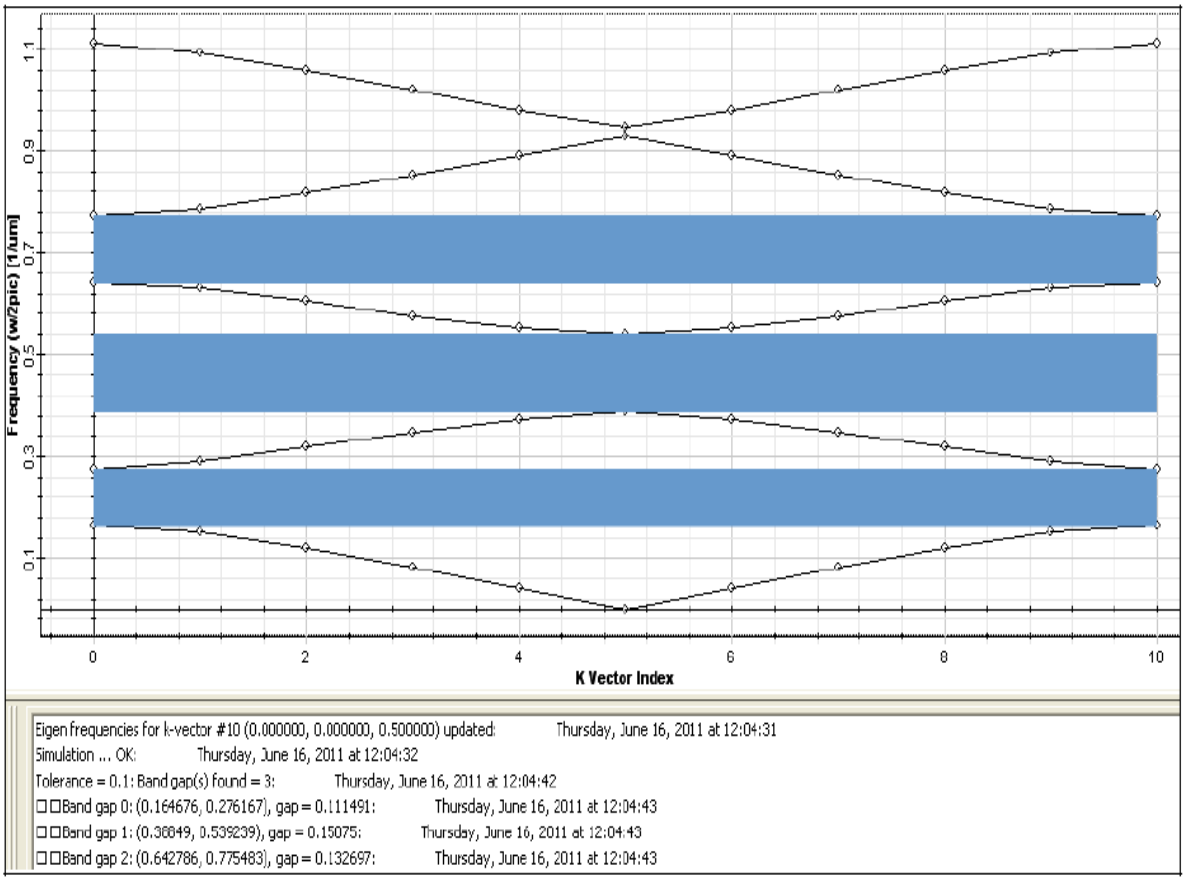

Figure 4.b Band structure of 1D binary PHC evaluated by Opti-FDTD simulator

VI. RESULTS AND DISCUSSIONS

5.1 BAND STRUCTURE AT 300K

At first, the bandgaps are evaluated at 300K by varying the angle of incidence from 0°-32°.

Table 1. Bandgaps of binary PHC at various angle of incidence at T=300K

ANGLE(°)	Bandgap 1(nm)	Bandgap 2(nm)	Bandgap 3(nm)	Bandgap 4(nm)
0	838-901	1048-1091	1289-1557	1846-2609
5	837-899	1046-1090	1287-1556	1843-2608
10	836-894	1039-1088	1280-1553	1837-2604
15	833-886	1028-1085	1269-1549	1826-2598
20	829-875	1013-1081	1255-1543	1811-2589
25	824-860	994-1075	1237-1536	1793-2579
30	819-840	970-1069	1217-1528	1792-2566

Table 2. Bandgaps of ternary PHC at various angle of incidence at T=300K

ANGLE(°)	Bandgap1 (nm)	Bandgap2 (nm)	Bandgap3 (nm)	Bandgap4 (nm)	Bandgap5 (nm)	Bandgap6 (nm)	Bandgap7 (nm)
0	855-890	970-981	1086-1126	1233-1336	1451-1645	1796-2121	2375-2959
5	854-889	969-980	1084-1126	1232-1335	1449-1664	1794-2120	2373-2958
10	853-886	968-975	1079-1124	1227-1334	1445-1642	1790-2118	2368-2955
15	851-881	965-969	1071-1122	1220-1331	1439-1639	1783-2113	2360-2949
20	849-873	957-964	1061-1118	1210-1327	1430-1634	1774-2107	2349-2941
25	845-862	944-960	1048-1114	1199-1322	1419-1628	1763-2100	2336-2931
30	841-848	928-956	1033-1109	1186-1317	1408-1622	1750-2092	2320-2920

Table (1) shows the bandgaps for binary PHC while **Table (2)** shows for the ternary PHC. In a ternary PHC due to Bragg scattering from two surfaces, the probability of destructive interference with the incoming wave is more compared to binary PHC. Thus a ternary PHC is expected to exhibit greater number of bandgaps. For a binary PHC we have only 4 bandgaps compared to 7 bandgaps for ternary PHC. This makes the ternary PHC more versatile in usage as we can choose wider range of wavelengths to work with.

5.2 BANDGAP AT 0° INCIDENCE ANGLE AND VARYING TEMPERATURE

In this section we evaluate the bandgaps by keeping the angle of incidence at 0° and varying the temperature from 100K-700K.

Table 3. Bandgaps of binary PHC at 0° incident angle. Temperature varies from 100K-700K

TEMPERAURE(K)	Bandgap 1(nm)	Bandgap 2(nm)	Bandgap 3(nm)	Bandgap 4(nm)
100	831-896	1044-1081	1282-1542	1832-2586
200	834-898	1046-1086	1285-1549	1839-2597
300	838-901	1048-1091	1289-1557	1845-2609
400	841-903	1051-1096	1293-1564	1852-2621
500	845-906	1053-1101	1296-1571	1859-2633
600	849-908	1055-1106	1300-1578	1866-2645
700	853-910	1057-1111	1304-1585	1873-2657

Table 4. Bandgaps of ternary PHC at 0° incident angle. Temperature varies from 100K-700K

Temp (K)	Bandgap1 (nm)	Bandgap2 (nm)	Bandgap3 (nm)	Bandgap4 (nm)	Bandgap5 (nm)	Bandgap6 (nm)	Bandgap7 (nm)
100	844-882	959-972	1077-1112	1221-1320	1436-1624	1775-2095	2348-2921
200	849-886	961-974	1081-1119	1227-1328	1443-1634	1785-2107	2354-2930
300	855-890	970-981	1086-1126	1233-1336	1451-1645	1796-2121	2375-2959
400	861-895	977-986	1090-1134	1240-1345	1459-1657	1807-2136	2390-2986
500	866-899	983-990	1095-1141	1246-1354	1467-1667	1817-2149	2404-2999
600	871-902	987-993	1099-1147	1251-1361	1251-1361	1473-1676	1826-2160
700	874-904	991-995	1101-1151	1254-1365	1254-1365	1477-1681	1831-2167

From Table 3 and Table 4, it is seen that the width of the bandgaps of the binary PHC increases with the rise of temperature except for the Bandgap 1 while the width of the bandgaps decrease with rise in temperature for the ternary PHC. With the decrease of width of the bandgap, the rejection capacity of a filter increases as it shows a sharper roll off. As a result we can reject one wavelength with more accuracy.

5.3 Perfromace Comparison As Dynmic Filter At T=300k

Suppose a bandgap extends from x1nm - x2 nm. The central forbidden wavelength is most tightly bound within the crystal i.e. (x1+x2)/2. So, the central forbidden wavelength is most easily filtered out by a PHC. In our case the solution to Equation (16) is obtained by considering a=Cos(t) where a=0.5(m11+m22) as found from Equations (6,9,10,12). $|a| \geq$ leads bandgap formation. At mid bandgap |a| is the greatest and |a|-1 gives the rejection factor(RF). The greater the rejection factor, easier it is to filter out the wavelength by the PHC. Refractive index of InAs and GaAs was evaluated first at T=300K and d1=d2=d3=500nm (at room temperature).

Table 5. Evaluation of rejection factors (RF) at various angle of incidence For binary PHC at T=300K. RF(i) stands for rejection factor of band(i)

Angle (°)	RF 1	RF 2	RF 3	RF 4
0	0.204873	0.040665	0.539274	0.766201
5	0.19373	0.04386	0.548019	0.770576
10	0.182775	0.054327	0.572303	0.783008
15	0.15559	0.074774	0.61323	0.803676
20	0.117297	0.109970	0.673479	0.833729
25	0.07193	0.167861	0.755892	0.871884
30	0.027153	0.259004	0.861745	0.919418

Table 6. Evaluation of rejection factors (RF) at various angle of incidence For ternary PHC at T=300K. RF(i) stands for rejection factor of band(i)

Angle(°)	RF1	RF2	RF3	RF4	RF5	RF6	RF7
0	0.201001	0.01096	0.101976	0.389937	0.716783	0.823713	0.74991
5	0.194668	0.009012	0.10786	0.3988457	0.725513	0.829088	0.752968
10	0.174481	0.004898	0.12684	0.425804	0.750641	0.845268	0.761812
15	0.141343	0.00135	0.090751	0.472912	0.792814	0.873441	0.776839
20	0.096947	0.005211	0.219544	0.543003	0.854182	0.912467	0.797776
25	0.048195	0.027865	0.307427	0.639097	0.93512	0.962615	0.824314
30	0.008191	0.086458	0.435923	0.765067	1.036356	1.04441	0.856457

By comparing Tables(1&5) for binary PHC and Tables(2&6) for ternary PHC, it can be concluded that from 820nm-900nm the rejection capability of binary PHC is superior compared to ternary PHC. From 900nm, the rejection factor of ternary PHC is superior to binary PHC. So, if we have to filter out any wavelength within the range of 820nm-900nm, then one should opt for binary PHC, after which ternary PHC is preferred due to higher rejection factor.

5.4 Performance Comparison As Temperature Sensor At 0° Incident Angle

The circuit used for temperatures sensing in [12] is shown in Figure 5. (W) is the central wavelength in a bandgap. Ideally, the optical power transmitted should be zero but in practice there is a finite value of transmitted power. But the power transmitted is certainly the least among all the wavelengths within the bandgap.

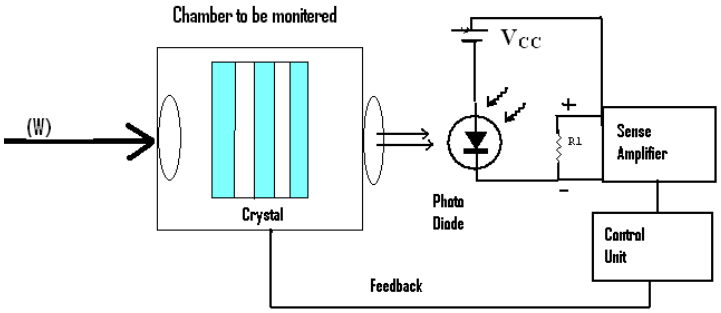

Fig. 5. Temperature sensor using photonic crystal. (W) Is the central bandgap wavelength. With variation of temperature (W) shifts from central bandgap location causing change in optical power transmitted.

Considering a binary crystal, let us suppose the temperature is 700K and we are working in the third bandgap. The temperature needs to be maintained at 700K. Then from Table 3 we get 1444.5nm as the central forbidden wavelength (W) of bandgap#3. The optical power transmitted by 14445.5 nm is the least among all the wavelengths in that bandgap. Inspection of Tables 3 and 4 reveal that with increase of temperature the central bandgap wavelengths of each bandgap tends to reach a higher value and vice versa for decrease of temperature.

So, if the temperature shifts from 700K, 1444.5 nm is no longer the central forbidden wavelength and thus the optical power transmitted by the photonic crystal increases which in turn increases the photoc current generated by the photo diode. This increase in photo current is detected by the sense amplifier which measures the small incremental change in potential difference across the photo diode.

Based on the findings of the sense amplifier the control unit can be used to raise an alarm to indicate that the temperature variation has gone beyond permissible limits.

The above circuit requires that the rejection factor at the mid forbidden bandgap should be as high as possible. The greater the rejection factor at mid bandgap, the better is the temperature sensing. In this section we evaluate the rejection factor at mid wavelength of the bandgaps of binary and ternary PHC. The changes due to variations of refractive index and lattice dimensions were incorporated for each point of evaluation. The incident angle was kept at 0° and temperature was varied from 100K-700K at intervals of 10K.

Table (7) and **Table (8)** shows the rejection factors of binary and ternary PHC respectively at some discrete temperature points. Detailed analysis of data shows that in general, the binary PHC performs as a better temperature sensor if the working range is within 840-1100nm. Within this range the rejection factors at central wavelengths of different bandgaps of ternary PHC gives lower values compared to its binary counterpart. After 1100nm the scenario is vice versa. So, if we are working with wavelengths in the range of 840-1100nm, then we should opt for binary PHC after which the ternary PHC gives better performance

Table 7. Rejection factors (RF) of binary PHC at 0° incident angle and temperature swing from 100K-300K. RF (i) gives |a|-1 at mid forbidden wavelength of bandgap #(i)

Temperature (K)	RF1	RF2	RF3	RF4
100	0.222341	0.031717	0.517819	0.755303
200	0.213628	0.036034	0.529114	0.76705
300	0.204873	0.040665	0.539842	0.76201
400	0.19609	0.045543	0.551654	0.77123
500	0.182618	0.050696	0.564353	0.779595
600	0.178234	0.055242	0.575708	0.784949
700	0.16948	0.062103	0.587134	0.789909

Table 8. Rejection factors (RF) of ternary PHC at 0° incident angle and temperature swing from 100K-300K. RF(i) gives |a|-1 at mid forbidden wavelength of bandgap #(i)

Temp(K)	RF1	RF2	RF3	RF4	RF5	RF6	RF7
100	0.23328	0.019617	0.077707	0.356937	0.680974	0.805703	0.738307
200	0.218102	0.015108	0.088527	0.372302	0.697533	0.814329	0.743262
300	0.201001	0.01096	0.101976	0.389937	0.716783	0.823253	0.74991
400	0.183255	0.007346	0.116646	0.407362	0.726611	0.831687	0.756204
500	0.167939	0.004846	0.130827	0.423836	0.754063	0.840009	0.761686
600	0.15547	0.003994	0.142709	0.438506	0.767541	0.846836	0.765524
700	0.147801	0.002192	0.150414	0.450514	0.774886	0.853136	0.76712

VI. CONCLUSION

A comparative study has been performed between binary and ternary PHC in respect of their dynamic optical filtering and temperature sensing performances. Chebyshev polynomials and Caley-Hamilton theorem was the backbone of the mathematical formulation. The band structure predicted by our model agrees to a good extent with the band structure generated by the Opti-FDTD 10.0 software which uses FDTD method to construct band structure. The study was restricted within 800-4000nm and 100K-700K. With temperature change, the variations due to change in refractive index, thermal coefficient of expansion and lattice dimensions were incorporated in master equation to get accurate results. At constant temperature the selective rejection capacity of ternary PHC was superior to binary PHC. The dynamic tuning performance at constant temperature by binary PHC was superior to ternary over 820nm-900 nm after which the ternary PHC performs better. As a temperature sensor the binary PHC performs better within the range of 840-1100nm after which the rejection factor of ternary PHC at central bandgap wavelength is higher compared to its binary counterpart. Our model is useful whenever one needs to design a dynamic optical tuner (as in optical amplifier) or using PHC as a temperature sensor in diversified applications.

ACKOWLEDGMENT

We are thankful to Prof. K.K.Ghosh who first introduced us into this ever interesting line of photonics. We are also indebted to Prof. A. Chakraborty for helping us in the mathematical aspects and giving us valuable references to enhance our understanding.

REFERENCES

[1]. Yabnolonovitch, E., "Inhibited spontaneous emission in solid state physics and electronics", Phys. Rev. Lett, APS, Vol.58(20), 2059-2062, 1987
[2]. Yablonovitch, E., "Photonics bandgap structures", JOSA B, Vol.10, 283-295, 1993
[3]. John, S., "Strong localization of photons in certain disordered dielectric superlattices", Phys. Rev.Lett, APS, Vol. 58(23), 2486-2489, 1987
[4]. Joannopoulous,J.D., Johnson,S.G., Winn,J.N. and Meade,R.D., [Photonic crystals, Molding the flow of light], Princeton University Press, Princeton, 2-5, 2008
[5]. Dekker,A.J., [Solid State Physics], Macmillan India Ltd, New Delhi, 238-242, 2006
[6]. Zhang,X.F., Shen,L.F., Wu,J.J. and Yang,T.J., "Backward guiding of terahertz radiation in periodic dielectric waveguides", Journal of Electromagnetic Waves and Applications, Vol.24, 557-564, 2010
[7]. John,S., "Theory of photonic bandgap materials", NATO ASI Series(E), Applied Science, Vol.315, 563-566, 1996
[8]. Ozbay,E., Temelkunran,B. and Bayindir,M., "Microwave applications of photonic crystals", PIER,Vol.41, 185-209, 2003
[9]. Wu,C.J., Liu,C.L.and Kuo,W.K., "Analysis of thickness dependant optical properties in a one dimensional superconducting photonic crystals", Journal of Electromagnetic Waves and Apllications,Vol.23, 1113-122, 2009
[10]. Srivastava,R., Pati,S. and Ojha,S.p., "Enhancement of omnidirectional reflection in photonic crystal heterostructures", PIER B, Vol.1, 197-208, 2008
[11]. Awasthi,S.K., Malaviya,U. and Ojha,S.P, "Enhancement of omnidirectional total reflection wavelength range by usinf one dimensional ternary phtonic bandgap material", JOSA B, Vol.23, 2566-2571, 2008
[12]. Lahiri,A. and Chakraborty, M., "Mathematical modeling of 1D binary photonic tuner and realization of temperature sensor", Proc, SPIE 8120,81200N (2011)
[13]. Born,M. and Wolf,E., [Principles of Optics], Cambridge University Press, U.K, 1-70, 1980
[14]. Glazov,V.M. and Pashinkin,A.S., "Thermal expansion and heat capacity of GaAs and InAs", Inorganic Materials, Vol.36(3), 225-231, 2000
[15]. Gillen,G.D., Di Rocco,C., Powers,P. and Guha,S., "Temperature dependant refractive index measurements of wafer shaped InAs ans InSb", Applied Optics, Vol.47(2), 2008
[16]. Ghosh,G., [Handbook of Thermo-Optic Coefficients of Optical Materials with Applications], Academic Press, U.K. , 1998
[17]. OptiFTD Ver.10, OptiFDTD_10_Technical_Background_and_Tutorials.pdf, pp. 263

APPENDIX

Expansion of total transfer characteristics matrix M(N(d))

This section deals with the proof of Equation 14.

Let us consider a matrix

$$A = \begin{pmatrix} m_{11} & m_{12} \\ m_{21} & m_{22} \end{pmatrix}$$

The characteristics equation for matrix A is given by

(λ-m11)(λ-m22)-m12m21=0, where λ is the eigen value for (A)

=>λ2- λ(m11+m22)+ det(A)=0

=> λ2- λ(m11+m22)+ 1=0 [substituting value of det(A)=1]

=>, λ2- 2aλ +1=0, where a=0.5(m11+m22)=0.5Tr(A)

=> λ= a ± i*(1-a2)0.5 …(A.I)

Let us take a=cosθ. Then the two solutions of equation(A.1) are given by λ1=exp(iθ) and λ2=exp(-iθ).

We need to proof that if (λ) is the eigen value of matrix (A), then the eigen value for the matrix (AN) is given by (λN).

Proof.

AX= λX, where (X) is the eigen vector and (λ) is the eigen value

Or, A2X= λAX

Or, A2X= λ2X

Or, A3X=λ2AX

Or, A3X=λ3X

Or, ANX= (λN)X

So ,we can conclude that (λN) is eigen value of matrix (AN).

So ,we see that (λN) is eigen value of matrix (AN).

Let us take P(λ) and Q(λ) as two polynomials of degree N and 2 respectively. Then P(λ) can be represented as P(λ)=Q(λ)q(λ)+ r(λ), where q(λ) is the quotient polynomial and r(λ) is the remainder ploynomial. If Q(λ) is the characteristic polynomial of matrix(A) then Q(λ)=0. So, we get P(λ)=r(λ). Since the degree of Q(λ) is 2, so the degree of r(λ) is 1.

So, λN=a1 λ+a0 , where P(λ)= λN and r(λ)= a1 λ+a0

=>from Cayley-Hamilton theorem(i.e. A matrix satisfies its own characteristics equation),

AN= a1A+ a0I ….(A.II)

Substituting two values of(λ), we get

λ1N=a1 λ1+a0 ..(A.III)

λ2N=a1 λ2+a0 .. (A.IV)

Solving equations (A.III) and (A.IV) we have

$$a_1 = Sin(N\theta) \Big/ Sin\theta$$

$$a_0 = -(\frac{Sin(N-1)\theta}{Sin\theta})$$

According to Equation A.II we have

$$A^N = \frac{SinN\theta}{Sin\theta}\begin{pmatrix} m_{11} & m_{12} \\ m_{21} & m_{22} \end{pmatrix} - \frac{Sin(N-1)\theta}{Sin\theta}\begin{pmatrix} 1 & 0 \\ 0 & 1 \end{pmatrix} \quad \text{…..(A.V)}$$

So,

$$or,\ A^N = \begin{bmatrix} m_{11}\dfrac{sinN\theta}{\sin\theta} - \dfrac{\sin(N-1)\theta}{\sin\theta} & m_{12}\dfrac{sinN\theta}{\sin\theta} \\ m_{21}\dfrac{sinN\theta}{\sin\theta} & m_{22}\dfrac{sinN\theta}{\sin\theta} - \dfrac{\sin(N-1)\theta}{\sin\theta} \end{bmatrix}$$

On substituting θ=Cos-1 a we get,

AN = M(N(d)) =

$$\begin{pmatrix} m_{11}U_{N-1}(a) - U_{N-2}(a) & m_{12}U_{N-1}(a) \\ m_{21}U_{N-1}(a) & m_{22}U_{N-1}(a) - U_{N-2}(a) \end{pmatrix}$$

This concludes our proof.